Supplementary Materials

Electrochemical Characterization of $ZnCl_2$ in NaCl-KCl and LiCl-KCl for Application to Zn Electrorefining from Zn-Ni Alloys

Carlos Mejia[1,], Hunter Manner[1], Jarod Varga[1], and Devin Rappleye[1]*

[1] Department of Chemical Engineering, Brigham Young University, Provo, Utah 84602 USA

* Corresponding author: carlos.mejia@byu.edu

This file includes:

Text S1. Determination of WE surface area and diffusion coefficient from CV

The electrochemically active surface area of the cylindrical W working electrode (WE, 1.5 mm diameter) was determined in both NaCl-KCl-$ZnCl_2$ at 973 K and LiCl-KCl-$ZnCl_2$ at 773 K by varying the immersion depth of the WE in the molten salt. A fixed scan rate (0.10 V s^{-1}) was used, and a cyclic voltammogram was recorded at each vertical position controlled by the translator. The cathodic peak current of Zn^{2+} reduction was measured at each depth and plotted as a function of the vertical translator position. The peak current increased linearly with position, consistent with uniform wetting of the cylindrical electrode surface. A least-squares linear fit of peak current versus position was used to determine the position at which the extrapolated current is zero, corresponding to the molten salt surface. The difference between this intercept and the final position gives the immersed length of the electrode. The effective electroactive area was then calculated from the geometric relation, A = $\pi dL + \pi(\frac{d}{2})^2$, where d is the electrode diameter and L is the immersed length. Using this approach, the exposed areas were 0.619 ± 0.0179 cm^2 in NaCl-KCl and 0.419 ± 0.0178 cm^2 in LiCl-KCl, consistent with the linear trends shown in **Figures S1** and **S9**.

The diffusion coefficient of Zn^{2+} from CV was obtained using the Berzins-Delahay expression for reversible metal deposition on a planar electrode.[1] For a diffusion-controlled reversible process, the cathodic peak current i_p is related to the scan rate v by

$$|i_p| = 0.6105nFAC_0^* \left(\frac{nFDv}{RT}\right)^{1/2} \qquad \text{(Eq. S1)}$$

where n is the number of electrons transferred (here $n = 2$ for the Zn^{2+}/Zn couple), F is Faraday's constant, A is the WE area determined as described above, C_0^* is the bulk concentration of Zn^{2+} in mol cm^{-3}, R is the gas constant, T is the absolute temperature, D is the diffusion coefficient, and v is the scan rate. For each molten salt system, the absolute value of the cathodic peak current from the fourth, iR-compensated scan was plotted as a function of $v^{1/2}$, and the data were fit with a straight line constrained to pass through the origin. The slope of this fit, $S = |i_p|/v^{1/2}$, was then used to calculate the diffusion coefficient by rearranging Equation (S1):

$$D = \frac{RT}{0.6105^2 n^3 F^3 A^2 (C_0^*)^2} S^2 \qquad \text{(Eq. S2)}$$

Equation S2 was applied using $T = 973$ K for the NaCl-KCl experiments and $T = 773$ K for the LiCl-KCl experiments, with the corresponding values of A and C_0^* for each system. The concentration of $ZnCl_2$ in NaCl-KCl and LiCl-KCl was 1.047 ± 0.099 × 10^{-4} mol cm^{-3} and 1.761 ± 0.125 × 10^{-4} mol cm^{-3}, respectively. The resulting diffusion coefficients obtained from CV data are reported in **Tables 1** and **4** of the main manuscript, along with the standard errors incorporating errors from concentration and area.

Text S2. Extraction of solution resistance from EIS measurements

Electrochemical impedance spectroscopy (EIS) was used to determine the uncompensated solution resistance, R_s, of each molten salt composition prior to voltammetric and transient measurements. For NaCl-KCl containing $ZnCl_2$, EIS was recorded at 0 V versus open circuit potential (OCP) over a frequency range of 0.1 MHz to 100 Hz using a small-amplitude sinusoidal perturbation. The Nyquist and Bode plots were inspected to confirm linear behavior. The spectra were fit with an equivalent circuit consisting of an inductive element in series with the solution resistance and a parallel combination of the double-layer capacitance and a charge-transfer branch containing a Warburg:

$$L - R_s - [C_{dl}||(R_{ct} - W)] \qquad \text{(Eq. S3)}$$

The intercept of the high-frequency semicircle with the real axis in the Nyquist plot corresponds to R_s. Fitted values for NaCl-KCl-$ZnCl_2$ gave $R_s = 0.177\ \Omega$, as reported in **Figure S2**.

For LiCl-KCl containing $ZnCl_2$, EIS was collected at 0 V versus OCP between 0.1 MHz and 10 Hz with identical perturbation amplitude. The same equivalent circuit was used to fit the spectra, yielding solution resistances near 0.32-0.33 Ω (**Figure S10**). For the LiCl-KCl electrorefining (ER) runs, the VIONIC potentiostat's built-in high-frequency impedance feature was used to estimate R_s automatically at 30 kHz with a 10 mV amplitude. These values were used for iR compensation of applied potentials and for calculating the actual potential, $E_{\text{actual}} = E_{\text{applied}} - iR_s$, in the main manuscript.

Text S3. Determination of the number of electrons from SWV

The number of electrons exchanged in the Zn^{2+}/Zn couple was obtained from SWV using the metal-deposition model of Fatouros and Krulic in the iR-compensated form of Fuller et al.[2] SWV was recorded with a step of −5 mV, an amplitude of 20 mV, and frequencies between 5 and 50 Hz. Potentials were actively compensated for solution resistance based on the value from EIS measurement. For each curve, the Zn^{2+} reduction peak was isolated, and the width of the second half of the peak at half height, w_2, was measured. The peak potential was first located, then the potential on the more negative side of the peak at half of the peak current was obtained by linear interpolation; w_2 is the difference between these two potentials. The pulse duration was calculated as $\Delta t = 1/(2f)$. Values of w_2 were plotted versus $\Delta t^{1/2}$. The frequency range where w_2 was approximately constant indicates the regime where nucleation and convection effects were minimal. The average w_2 over this plateau region was used in all iR-compensated Fatouros-Krulic relation[3]

$$w_2 = W_2 \frac{RT}{nF} \qquad \text{(Eq. S4)}$$

where R is the gas constant, T is temperature, F is Faraday's constant, and W_2 is a dimensionless peak-shape parameter. Following Fuller et al., $W_2 = 0.91$ was adopted for well-compensated molten salt conditions. The number of electrons was then calculated from

$$n = W_2 \frac{RT}{Fw_2} \quad \text{(Eq. S5)}$$

In both NaCl-KCl and LiCl-KCl molten salts, the resulting values of n were close to 2, confirming a two-electron Zn^{2+}/Zn process.

Text S4. Chronoamperometry and Cottrell analysis

Chronoamperometry (CA) was used to obtain diffusion coefficients of Zn^{2+} in both molten salt systems by applying short potential steps close to and beyond the Zn^{2+}/Zn reduction peak. After each step, the current transient was recorded for 2 s, followed by an oxidative cleaning step and a relaxation period at OCP. The analysis is based on the Cottrell relation for a planar electrode with semi-infinite linear diffusion:[4]

$$i(t) = \frac{nFAC^* D^{1/2}}{\pi^{1/2} t^{1/2}} \quad \text{(Eq. S6)}$$

where $i(t)$ is the current at time t, and symbols have their usual meaning.

For each potential, the negative current was plotted as $\ln(-i)$ versus $\ln(t)$. In an ideal diffusion-controlled regime, the slope of this log-log plot is expected to be −0.5. The intercept is related to $nFAC^* D^{1/2}/\pi^{1/2}$. Representative plots for NaCl-KCl-$ZnCl_2$ at 973 K and LiCl-KCl-$ZnCl_2$ at 773 K are shown in **Figures S3** and **S11**, respectively.

In NaCl-KCl, the fitted slope was −0.349 with a correlation coefficient of 0.965, indicating significant deviation from Cottrell behavior. Hence, the reliability of D is questionable when calculated from CA data in NaCl-KCl. The deviation from −0.5 is likely due to the higher temperature, increased convection, and small contributions from double-layer charging that are more pronounced at 973 K. In contrast, the LiCl-KCl system gave a slope of −0.473 with an R^2 of 0.9996, very close to the ideal −0.5, consistent with diffusion-controlled Zn^{2+} reduction at 773 K.

For each potential step, the diffusion coefficient was extracted from the fitted intercept. **Tables S1** and **S4** summarize the applied potentials, the slopes, the intercepts, and the resulting diffusion coefficients, with reported errors that incorporate the errors from the concentration and area in NaCl-KCl and LiCl-KCl, respectively. For CA analysis in LiCl-KCl, the $ZnCl_2$ concentration was $1.283 \pm 0.037 \times 10^{-4}$ mol cm^{-3}. The exposed area was 0.654 ± 0.0179 cm^2. The average CA-derived diffusion coefficients reported in the main manuscript were calculated as the mean across all potentials, along with the standard errors from the concentration and area.

Text S5. Chronopotentiometry, Sand's equation, and transition time analysis

Chronopotentiometry (CP) was used as an independent method to determine Zn^{2+} diffusion

coefficients using Sand's transition time analysis.[5] Constant cathodic currents were applied for a fixed duration to drive Zn deposition until the near-surface Zn^{2+} concentration approached zero. The potential response was recorded as a function of time, then the current was turned off and the system allowed to relax at OCP to obtain the Zn^{2+}/Zn redox potential.

To extract the transition time, τ, the time derivative of the potential, dE/dt, was calculated and plotted versus time. In a diffusion-controlled regime, the potential decreases gradually until the depletion of Zn^{2+} at the electrode surface, at which point dE/dt exhibits a sharp drop. The first inflection in dE/dt was taken as Sand's transition time, as illustrated in **Figures S4** and **S12** for NaCl-KCl and LiCl-KCl, respectively. In NaCl-KCl, τ was 1.0751 s at the selected current of −0.10 A; in LiCl-KCl, τ was 0.6461 s for a current of −0.05 A.

The diffusion coefficient was then obtained from Sand's equation for a planar electrode:

$$\tau = \frac{\pi D}{4}\left(\frac{nFC^*}{j}\right)^2 \qquad \text{(Eq. S7)}$$

where j is the applied current density. For each current step, τ was determined from the dE/dt analysis and substituted into Sand's expression to calculate D. **Tables S2** and **S5** list the applied currents, τ values, calculated diffusion coefficients along with the reported error from the concentration and area for NaCl-KCl and LiCl-KCl, respectively. The mean CP-derived diffusion coefficients reported in the main manuscript were obtained by averaging across all current steps for each salt system, incorporating errors associated with concentration and area.

Text S6. Definition and calculation of Faradaic efficiency and yield

ER performance was evaluated using Faradaic efficiency (FE) and yield. Both metrics were calculated separately for each ER run.

The cathodic FE describes how effectively the charge passed to the cathode was used to deposit Zn:

$$\mathrm{FE_{cathode}} = \frac{m_{\mathrm{Zn,cathode}} nF}{M_{\mathrm{Zn}} Q_{\mathrm{passed}}} \qquad \text{(Eq. S8)}$$

where $m_{\mathrm{Zn,\ cathode}}$ is the mass of Zn in the cathode product, M_{Zn} is the molar mass of Zn, $n = 2$ for the Zn^{2+}/Zn couple, and Q_{passed} is the total charge passed during the run. For NaCl-KCl, the cathode and anode products were dissolved and analyzed by ICP-MS to determine Zn and Ni contents, with SEM-EDX used qualitatively to confirm the absence of Ni in the cathode sample (**Figure S8**). For LiCl-KCl runs, cathode rings and anode heels were characterized by XRF.

The yield was defined as the fraction of the total Zn inventory recovered in the cathode product:

$$\mathrm{Yield} = \frac{m_{\mathrm{Zn,cathode}}}{m_{\mathrm{Zn,alloy}} + m_{\mathrm{Zn,salt}}} \qquad \text{(Eq. S9)}$$

where $m_{\mathrm{Zn,alloy}}$ is the initial mass of Zn present in the Zn-Ni anode alloy and $m_{\mathrm{Zn,salt}}$ is the mass of

Zn contributed by $ZnCl_2$ dissolved in the molten salt. This definition reflects the fact that some Zn remains in the anode heel at the end of the run, and a small fraction adheres to the tungsten ring or is lost during sample handling.

The anodic FE was evaluated based on the mass loss of Zn from the anode:

$$\mathrm{FE}_{\mathrm{anode}} = \frac{\Delta m_{\mathrm{Zn,anode}} nF}{M_{\mathrm{Zn}} Q_{\mathrm{passed}}} \qquad \text{(Eq. S10)}$$

where $\Delta m_{\mathrm{Zn,\ anode}}$ is the mass of Zn removed from the anode during the ER run. This value was estimated from the change in anode mass and the final Zn composition measured by XRF. Since XRF is a surface analysis technique, there is some uncertainty in the measured bulk composition, which can lead to deviations in the calculated anodic FE.

Tables S3 and **S6** list the starting compositions of the salt and anode metals, total charge passed, and run times for NaCl-KCl and LiCl-KCl ER experiments, respectively. These values were combined with post-run product masses to compute FE and yield for each case, which are summarized in the main text tables.

Text S7. Additional details on ER apparatus and thermal behavior

Supplementary figures provide additional information on the mechanical design of the ER setups, crucible configurations, and thermal behavior of salts and metals.

Figures S5 and **S14** show the alumina stirrer assemblies and electrode geometries used in the NaCl-KCl and LiCl-KCl runs. The NaCl-KCl experiments used a straight 1.5 mm W rod embedded in a custom alumina paddle to improve mixing while minimizing metal contact with the alumina support. For LiCl-KCl, the WE was modified to a W hook sheathed in an alumina paddle, and the counter electrode (CE) was fabricated as a W ring with a side cut to accommodate the RE in the annular gap.

Crucible configurations are shown in **Figure S15**. The NaCl-KCl ER run used MgO crucibles for both inner and outer containers. For LiCl-KCl, Run A utilized boron nitride inner and outer crucibles, while Run B used MgO crucibles with the same dimensions. The inner crucible contained the Zn-Ni anode metal, and the outer crucible housed the LiCl-KCl-$ZnCl_2$ salt and cathode ring. **Figure S16** shows the assembled ER apparatus, including the aluminum support frame, alumina-insulated current leads, and the lid with designated openings for the WE, CE, and RE.

Thermogravimetric and differential scanning calorimetry (TGA-DSC) were used to assess the volatility and melting behavior of Zn, $ZnCl_2$, and LiCl-KCl-$ZnCl_2$ mixtures. **Figure S7** presents TGA-DSC curves for Zn metal and $ZnCl_2$, showing that both species begin to lose mass significantly above roughly 873 K (600 °C), consistent with the sublimation behavior that complicates ER in NaCl-KCl. **Figures S6** and **S13** illustrate the practical consequences of this volatility, with condensed Zn metal observed in the cold regions of the NaCl-KCl ER apparatus and stable behavior

of LiCl-KCl-$ZnCl_2$ up to 873 K. These observations motivated the transition to LiCl-KCl for lower temperature ER.

References

(1) Berzins, T.; Delahay, P. Oscillographic Polarographic Waves for the Reversible Deposition of Metals on Solid Electrodes. *J. Am. Chem. Soc.* **1953**, *75* (3), 555–559. https://doi.org/10.1021/ja01099a013.

(2) Fuller, R.; Williams, T.; Schvaneveldt, M.; Rappleye, D. A Comparison of Square-Wave Voltammetry Models to Determine the Number of Electrons Exchanged in Metal Deposition. *Electrochim. Acta* **2022**, *414*, 140220. https://doi.org/10.1016/j.electacta.2022.140220.

(3) Fatouros, N.; Krulic, D. Contribution to the Study of Square Wave Voltammetry in the Case of Simple Irreversible Reactions. *J. Electroanal. Chem.* **1998**, *443* (2), 262–265. https://doi.org/10.1016/S0022-0728(97)00541-X.

(4) Cottrell, F. G. Residual Current in Galvanic Polarization Regarded as a Diffusiona Problem. *Z. Phys. Chem.* **1903**, *42* (1), 385–431. https://doi.org/10.1515/zpch-1903-4229.

(5) Sand, H. J. S. III. On the Concentration at the Electrodes in a Solution, with Special Reference to the Liberation of Hydrogen by Electrolysis of a Mixture of Copper Sulphate and Sulphuric Acid. *Lond. Edinb. Dubl. Phil. Mag.* **1901**, *1* (1), 45–79. https://doi.org/10.1080/14786440109462590.

Supplementary Figures

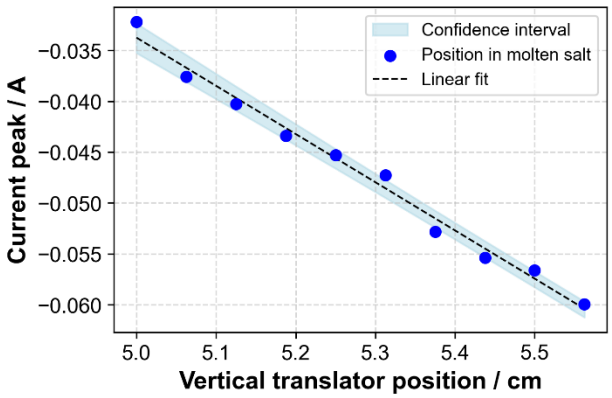

Figure S1. Determination of the WE surface area in NaCl-KCl at 973 K by measuring current as a function of the immersion depth of the electrode in the molten salt. The linear fit is y = −0.0474x + 0.2032, where y is the peak current and x is the electrode position. The x-intercept (i.e., y = 0, current is 0 A) is 4.287 cm. The final position of 5.562 cm was used for electrochemical measurements. This corresponds to an immersion depth of 1.275 cm. The effective surface area was found to be 0.619 cm^2. WE: 1.5 mm diameter W rod; CE: 3.175 mm diameter W rod; RE: Ni/NiO (1 mol%).

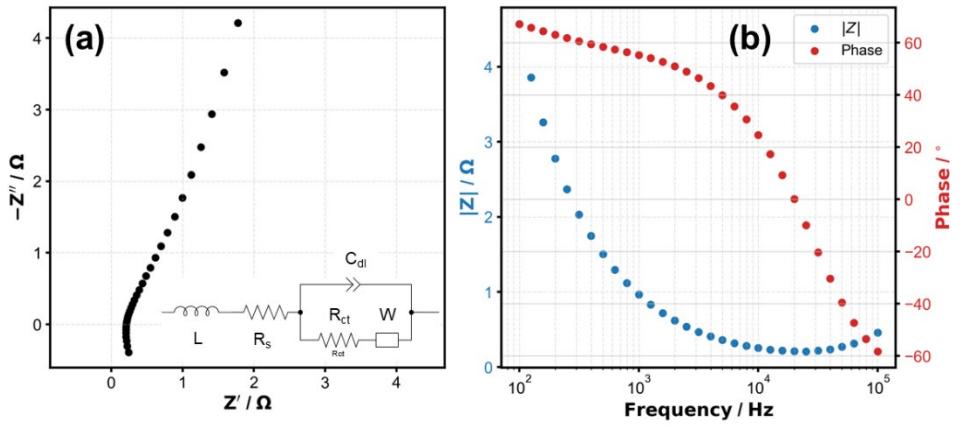

Figure S2. EIS measurement to determine the solution resistance in NaCl-KCl at 973 K. **(a)** Nyquist plot and **(b)** Bode plot acquired at 0 V versus OCP from 0.1 MHz to 100 Hz. The data in **(a)** were fitted using the equivalent circuit shown in the inset, yielding a solution resistance R_s of 0.177 **Ω**. WE: 1.5 mm diameter W rod; CE: 3.175 mm diameter W rod; RE: Ni/NiO (1 mol%).

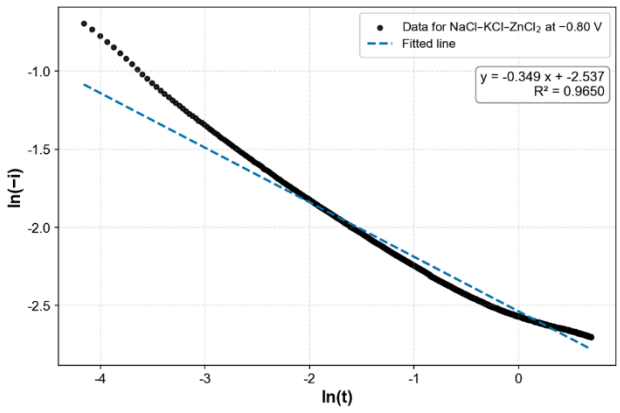

Figure S3. Cottrell behavior of NaCl-KCl-$ZnCl_2$ at 973 K. The natural logarithm of the negative current from CA experiments is plotted versus the natural logarithm of time. Black dots represent experimental data, and the blue dashed line is the linear fit, with the legend showing the regression equation (R^2 = 0.9650) and a slope of −0.349.

Table S1. Summary of CA parameters and the averaged diffusion coefficient for Zn^{2+} in NaCl-KCl at 973 K. Data are shown for five representative potentials from −0.56 to −0.80 V (0.01-0.02 V intervals), using a WE area A = 0.619 cm^2, and bulk $ZnCl_2$ concentration C_o^* = 1.047 × 10^{-4} mol cm^{-3}.

Applied Potential / V	Slope	Intercept	D (x 10^{-4}) / cm^2 s^{-1}
−0.56	−0.343	−2.618	1.069 ± 0.27
−0.60	−0.333	−2.538	1.257 ± 0.31
−0.68	−0.363	−2.572	1.173 ± 0.29
−0.74	−0.362	−2.568	1.182 ± 0.30
−0.80	−0.349	−2.538	1.257 ± 0.32
Average *D*			1.157 ± 0.29

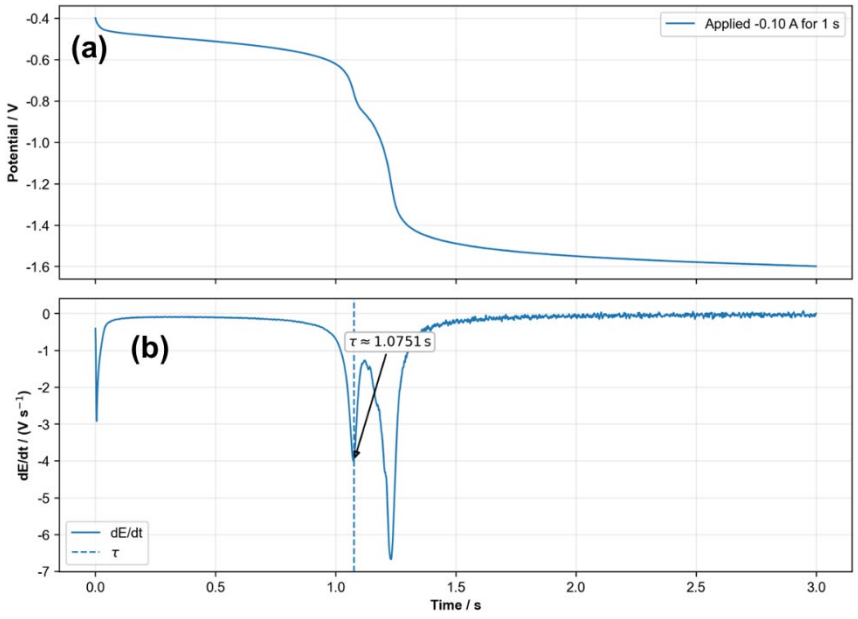

Figure S4. Determination of Sand's transition time (τ) for Zn^{2+} reduction in NaCl-KCl at 973 K using CP. **(a)** Measured CP potential transients, and **(b)** time derivative of the potential (dE/dt) versus time. The transition time τ is identified as the point of first deviation in dE/dt from its initial behavior, corresponding to the time when the Zn^{2+} concentration at the WE surface is depleted, and Zn deposition becomes diffusion-limited. The calculated τ is 1.0751 s.

Table S2. Summary of CP parameters and the averaged diffusion coefficient for Zn^{2+} in NaCl-KCl at 973 K. Current steps were 1 s. The WE area was 0.619 cm^2, and the bulk $ZnCl_2$ concentration was $C_o^* = 1.047 \times 10^{-4}$ mol cm^{-3}. τ denotes Sand's transition time.

Applied Current / A	τ / s	D (x 10^{-5}) / cm^2 s^{-1}
−0.10	1.075	8.765 ± 2.22
−0.12	0.781	9.173 ± 2.32
−0.14	0.594	9.494 ± 2.40
Average *D*		9.144 ± 2.31

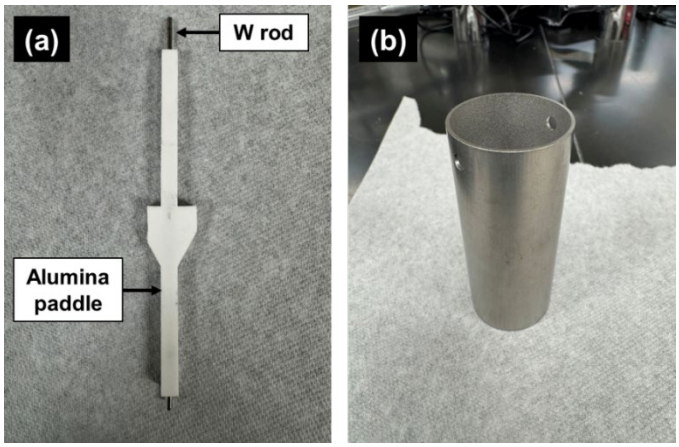

Figure S5. Photographs of the electrodes used for Zn ER in NaCl-KCl. **(a)** Alumina stirrer with a 1.5 mm diameter W rod; and **(b)** W ring used as the cathode in the ER run.

Table S3. Experimental conditions for Zn ER in NaCl-KCl at 973 K, including starting salt composition, initial anode metal composition, total charge passed, and total run time.

Starting salt composition						**Starting anode metal**				**Run results**	
NaCl		KCl		$ZnCl_2$		Zn		Ni		Charge Passed	Total time
/ g	/ mol%	/ g	/ mol%	/ g	/ mol%	/ g	/ at.%	/ g	/ at.%	/ C	/ h

39.65	47.97	49.59	47.04	9.63	4.99	55.33	98.0	1.01	2.0	249571	13.94

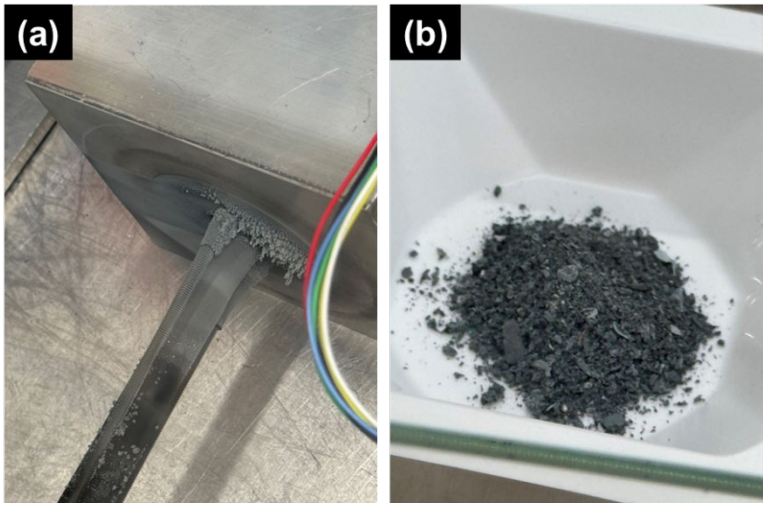

Figure S6. Zn metal sublimation products in the 100 g NaCl-KCl ER apparatus. **(a)** Deposited Zn metal in the colder region of the apparatus; and **(b)** Zn deposits collected after cleaning the apparatus.

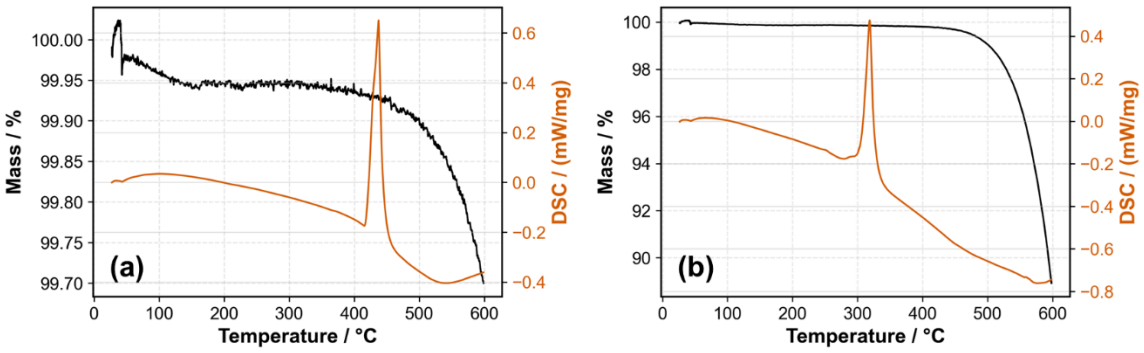

Figure S7. TGA-DSC data for **(a)** Zn metal and **(b)** $ZnCl_2$. The measured melting point of Zn is 690 K (417 °C), and the measured melting point of $ZnCl_2$ is 574.9 K (301.9 °C).

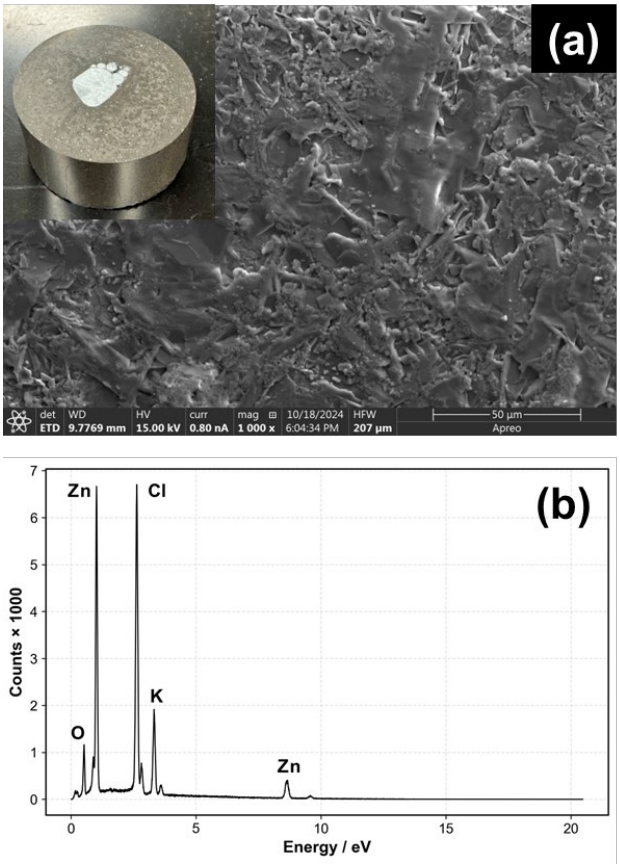

Figure S8. SEM-EDX characterization of the NaCl-KCl ER cathode product. **(a)** SEM image showing the cathode morphology, with an inset of the sample embedded in epoxy for cross-sectional analysis; and **(b)** EDX spectrum showing only Zn, Cl, K, and O signals, indicating the absence of Ni contamination in the cathode product.

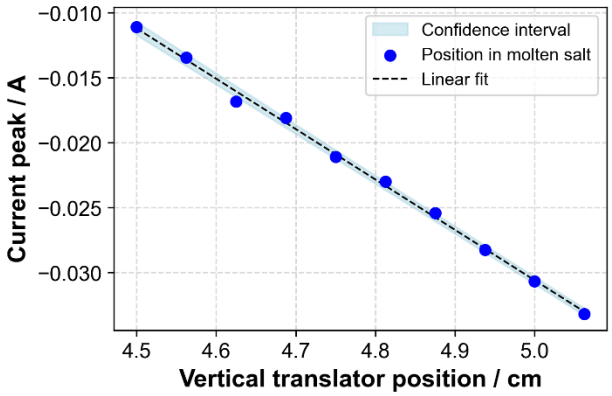

Figure S9. Determination of the WE surface area in LiCl-KCl-$ZnCl_2$ at 773 K. The peak current is plotted as a function of the vertical position of the WE rod in the molten salt to determine the immersed area (procedure analogous to **Figure S1** for NaCl-KCl-$ZnCl_2$). The linear fit is $y = -0.0388x + 0.1634$ with an immersion depth of 0.851 cm.

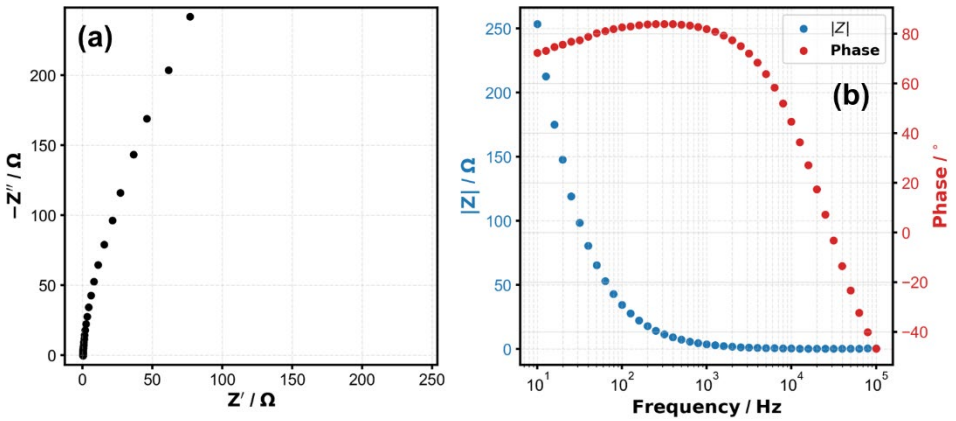

Figure S10. EIS measurement to determine the solution resistance of LiCl-KCl containing $ZnCl_2$ at 773 K. **(a)** Nyquist plot and **(b)** Bode plot acquired at 0 V versus OCP from 0.1 MHz to 10 Hz. The data were fitted with an equivalent circuit analogous to that used for the NaCl-KCl system, yielding a solution resistance of 0.323 Ω.

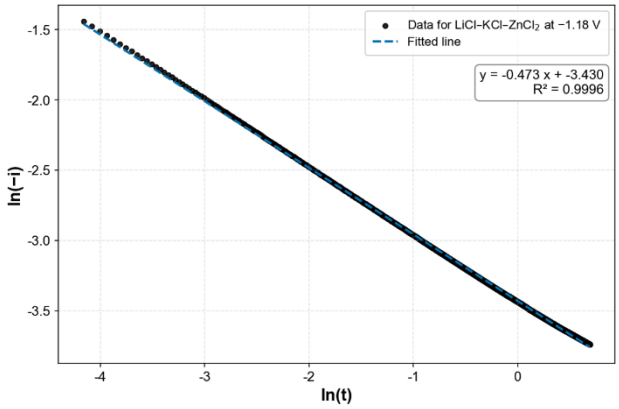

Figure S11. Cottrell behavior of LiCl-KCl-$ZnCl_2$ at 773 K. The natural logarithm of the negative CA current is plotted versus the natural logarithm of time. Black dots represent experimental data, and the blue dashed line is the linear fit. The legend shows the linear regression equation with $R^2 = 0.9996$ and a slope of −0.473.

Table S4. Summary of CA parameters and the averaged diffusion coefficient for Zn^{2+} in LiCl-KCl at 773 K. Five representative potentials from −0.98 to −1.18 V (0.01 V intervals) were used, with WE area A = 0.654 cm^2 and bulk $ZnCl_2$ concentration $C_o^* = 1.283 \times 10^{-4}$ mol cm^{-3}.

Applied Potential / V	Slope	Intercept	D (x 10^{-5}) / cm^2 s^{-1}
−1.05	−0.475	−3.459	1.184 ± 0.133
−1.08	−0.474	−3.456	1.193 ± 0.134
−1.12	−0.469	−3.433	1.249 ± 0.141
−1.15	−0.471	−3.434	1.246 ± 0.140
−1.18	−0.473	−3.430	1.256 ± 0.142
Average *D*			1.188 ± 0.134

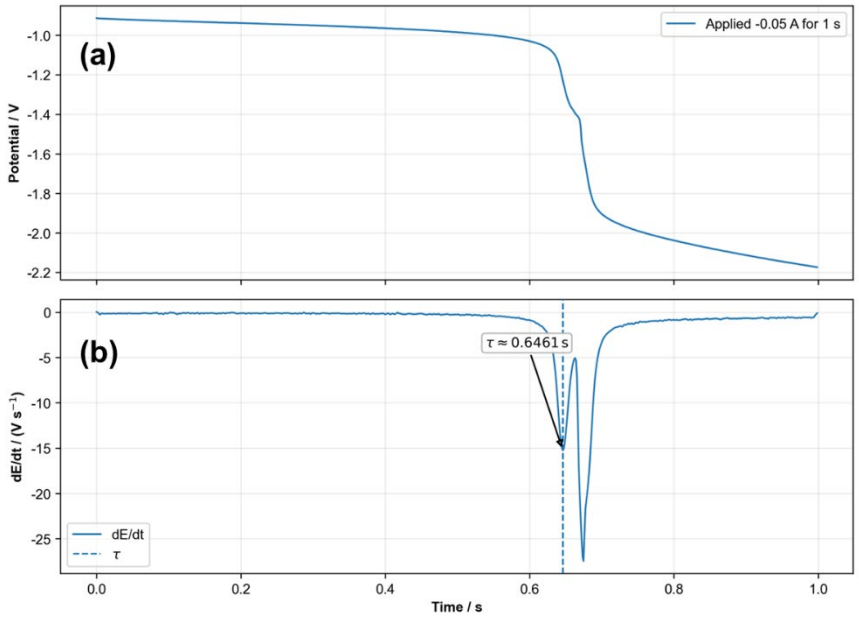

Figure S12. Determination of Sand's transition time (τ) for Zn^{2+} reduction in LiCl-KCl at 773 K using CP. **(a)** Measured CP potential transients; and **(b)** dE/dt versus time. The transition time τ is identified from the first deviation in dE/dt, corresponding to depletion of Zn^{2+} at the WE surface and the onset of diffusion-limited deposition. The calculated τ is 0.6461 s.

Table S5. Summary of CP parameters and the averaged diffusion coefficient for Zn^{2+} in LiCl-KCl at 773 K. Current steps were 1 s. The WE area was 0.419 cm^2, and the bulk $ZnCl_2$ concentration was $C_o^* = 1.761 \times 10^{-4}$ mol cm^{-3}. τ denotes Sand's transition time.

Applied Current / A	τ / s	*D* (x 10^{-5}) / cm^2 s^{-1}
−0.05	0.6461	1.015 ± 0.233
−0.07	0.3159	0.973 ± 0.224
−0.09	0.1833	0.933 ± 0.215
Average *D*		0.974 ± 0.224

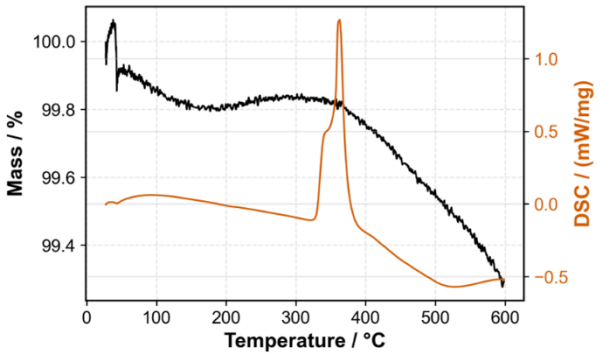

Figure S13. TGA-DSC data for a LiCl-KCl-$ZnCl_2$ salt block containing 96 mol% eutectic LiCl-KCl and 4 mol% $ZnCl_2$, showing a melting point of 602.3 K (329.3 °C).

Table S6. Experimental salt compositions for all Zn ER runs (Runs A and B) in LiCl-KCl-$ZnCl_2$.

Run	**Starting salt composition**					
Run #	LiCl		KCl		$ZnCl_2$	
	/ g	/ mol%	/ g	/ mol%	/ g	/ mol%
A	40.567	56.31	50.281	39.69	9.278	4.00
B	44.593	56.25	55.407	39.74	10.195	4.00

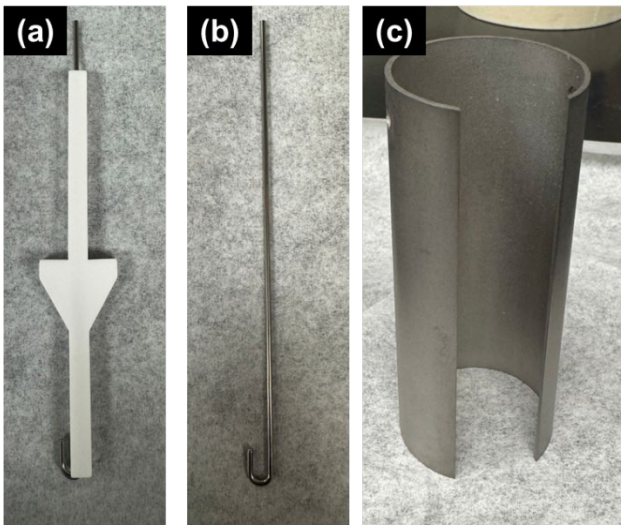

Figure S14. Photographs of the components used in the LiCl-KCl ER cell. **(a)** Alumina paddle used to isolate the W hook such that only the bottom of the hook contacts the molten salt; **(b)** W hook used as the WE; and **(c)** W cathode ring with a cut to accommodate placement of the RE during ER.

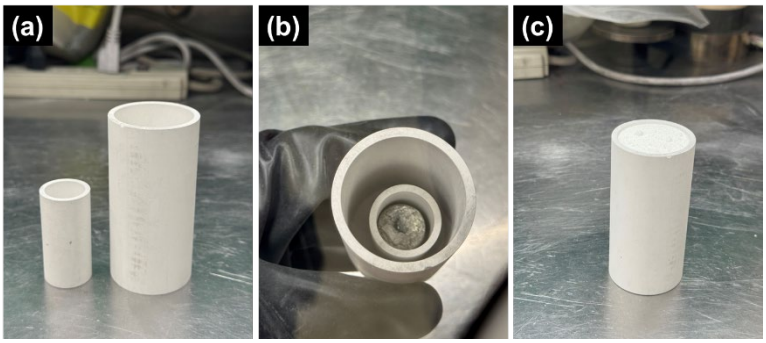

Figure S15. Crucible configurations for Zn ER in LiCl-KCl-$ZnCl_2$. **(a)** Inner and outer BN crucibles; **(b)** anode metal placed inside the inner crucible; and **(c)** addition of 100 g of salt containing 96 mol% eutectic LiCl-KCl and 4 mol% $ZnCl_2$. BN crucibles were used for Run A, while MgO crucibles of the same dimensions were used for Run B.

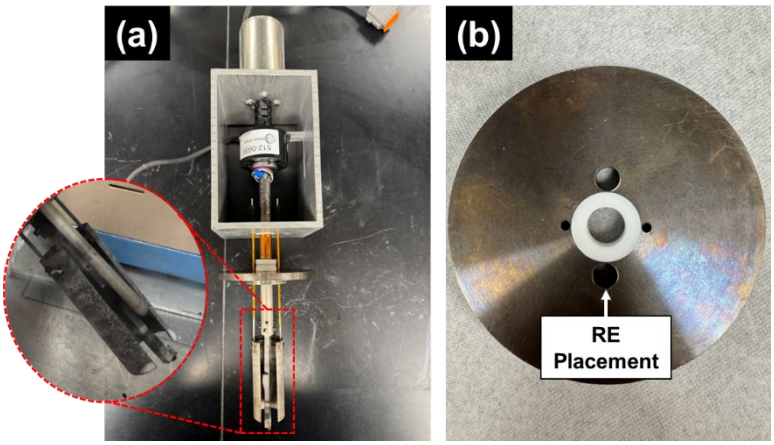

Figure S16. Photographs of the LiCl-KCl Zn ER setup. **(a)** ER assembly mounted outside the glovebox, showing the electrodes and mechanical connections; the cathode ring support rods are insulated with Kapton tape to prevent electrical contact with the alumina frame. The red-dashed inset highlights the location where the RE is introduced inside the glovebox. **(b)** SS316 lid assembly used to hold the electrodes, with one of the openings designated for the RE.